Polish Society of Composite Materials
Polskie Towarzystwo Materiałów Kompozytowych

24: 1 (2024) 25-32

COMPOSITES THEORY AND PRACTICE

ISSN (online): 2299-128X

Kalyanamanohar Veeramallu*, Alluru Gopala Krishna

JNTUK Kakinada, Department Mechanical Engineering, University College of Engineering Kakinada (A), 533003, Andhra Pradesh, India
**Corresponding author: E-mail: kalyanamanohar@jntucek.ac.in*

Received (Otrzymano) 05.10.2023

ENHANCED WEAR AND CORROSION PERFORMANCE OF STAINLESS STEEL 316L WITH ADDITION OF DIFFERENT WEIGHT PERCENTAGES OF GNP

https://doi.org/10.62753/ctp.2024.04.1.1

The present study reports on the significant improvement in the wear and corrosion resistance of SS316L by adding graphene nanoplatelets (GNP) of varying wt.% (0.25, 0.5, and 0.75), composites which were prepared by the pressureless sintering technique. The GNP addition can significantly improve the wear and corrosion resistance of SS316L. The wear and corrosion rates for the 0.5 wt.% GNP composite were reduced by 43% and 98%, respectively. The corrosion morphology showed that pitting corrosion was reduced by reinforcing 316L with 0.5 wt.% GNP. Moreover, the intergranular sites were more vulnerable to the corrosion medium when GNP was used at 0.75 wt.%. The worn surface morphology revealed that the tribofilm reduces the coefficient of friction and wear rate due to the lubricating nature of GNP. The presence of GNP was confirmed by Raman spectroscopy in terms of the tribofilm.

Keywords: stainless steel, 316L, morphology, corrosion rate, worn surface morphology

INTRODUCTION

Stainless steel 316L particularly, austenitic stainless steel, has become an active part of the constantly developing modern technology due to its corrosion resistance and customized mechanical properties. It finds numerous applications in automotive, structural, and biomedical fields. However, it exhibits moderate wear and corrosion resistance on account of its low hardness, which further limits the life of components made of this material. Many efforts have been made to increase the corrosion and wear performance of 316L. To improve resistance to corrosion and wear, different coatings i.e. diamond-like carbon [1] Ni-Cr [2] Co-Cr [3] have been applied. Another method to reinforce SS316L with a corrosion and wear-resistant material. Kuforiji et al. developed composites with 50 wt.% SS316L and 50 wt.% Al_2O_3 at the pressure of 794.4 MPa; subsequently, the liquid phase was sintered at 1400 °C for 1 hour. The inclusion of 50 wt.% aluminum oxide particles reduced the wear rate by 86% when compared to the base SS316L [4].

Padmavathi et al. [5] analyzed the addition of Y_2O_3 and yttrium aluminum garnet (YAG) to SS316L at 1200 °C and 1400 °C, 600 MPa for 60 min. The 316L-5YAG composite was found to be more corrosion resistant and achieved a high density at supersolidus temperature conditions. Mahathanabodee et al. added hexagonal boron nitride (h-BN) to 316L stainless steel by powder metallurgy at the sintering temperature of 1200 °C. The SS316L/20 wt.% h-BN composites achieved a better specific wear rate and coefficient of friction range of 0.3-0.4 [6]. Kumar et al. fabricated Y_2O_3/TiO_2 reinforced 304L stainless steel nanocomposites using mechanical alloying (MA). They reported that the hardness and wear resistance grew with the addition of nanoparticle reinforcement in a 304L steel matrix [7]. Zou et al. investigated the laser powder bed fusion (LPBF) of SiC-reinforced 316L stainless steel metallic matrix composites (MMCs) to improve the ultimate tensile strength and wear resistance. A 9 vol.% SiC addition greatly improves the ultimate tensile strength (1.3 GPa) and wear rate ($0.77x10^{-5}$ mm^3/Nm) of 316L [8]. Balaji et al. studied the effect of Fe_3Al and Ni_3Al additions to SS316L at supersolidus temperatures (1400°C). 316L with the addition of 5 wt.% Ni_3Al and Fe_3Al exhibited an improvement in the corrosion and wear resistance [9].

In recent years, some nanoreinforcements have been widely used in SS316L. These nanoreinforcements obstruct grain growth, thereby producing a refined grain structure, further enhancing the mechanical properties. Nanoreinforcements like carbon nanotubes (CNTs) and graphene nanoplatelets (GNP) have been incorporated into SS316L using diffe rent methods. Zengin et al. developed 316L/CNT stainless steel nanocomposites utilizing powder metallurgy (PM). They noticed that the hardness and wear resistance of the nanocomposites increased with a greater amount of CNTs as a consequence of better sintering conditions [10]. Radhamani et al.

reinforced 316L stainless steel (SS) with carbon nanotubes using the spark plasma sintering technique at 800 °C. A ball-on-disc tribometer was employed to examine the tribological behavior of 0.2, 0.5, 1.0, and 2.0 wt.% CNT/SS 316L samples at 28 °C and 300 °C under a load of 10 N. The microstructural investigations revealed grain refinement by the inclusion of CNTs, which improves the hardness and yield strength. The wear rate also decreased as the CNT content was increased [11].

The effect of different GNP wt.% additions to SS316L was presented in our previous publication [12]. However, the wear and corrosion characteristics of SS316L/GNP composites were not explored. This present study exclusively investigates the effect of GNP additions on the wear and corrosion properties of SS 316L.

EXPERIMENTAL PROCEDURE

In the present work, SS316L with a particle size of 45 µm as the matrix and GNP with a thickness of 3-5 nm as the reinforcement were taken to fabricate the composites. Initially, the desired weight fractions 100% SS316L, 99.5/0.5, 99.25/0.75 SS316L/GNP powders were ultrasonicated in an ethanol solution at 10 kHz in a probe sonicator for 1 h. Afterwards, the mixture was ground in a planetary ball mill (Labindia, BM 1100+, India), which was operated at 300 RPM, with ball-to-powder ratio of 10:1 for 2 h. Then the blended mixture was dried at 100 °C on a hot plate for 2 h. The ethanol in the milled mixture was evaporated and a fine powder was obtained. The milled composite powders were compacted at 600 MPa to prepare cylindrical specimens with a diameter of 20 mm and thickness of 6 mm for the corrosion test and specimens with a diameter of 10 mm and 15 mm in height for the wear test as shown in Figure 1. All the green SS316L, SS316L-GNP (0.25 wt.%, 0.5 wt.% and 0.75 wt.%) composite specimens were liquid phase sintered at 1400 °C in a vacuum furnace for a holding time of 90 min. The rule of mixture formula was used to calculate the theoretical densities of the composites. The sintered density of the specimens was measured using Archimedes' principle. The relative density was calculated by the ratio of bulk to theoretical density.

The corrosion tests for all the specimens were carried out on a 3-electrode electrochemical potentiostat (Metrohm Autolab, Netherlands) as per the ASTM G102-89 standard. Then 3.5 wt.% NaCl was used as the corrosive medium during the polarization test. In a 3-electrode electrochemical cell, silver/silver chloride (Ag/AgCl) was the reference electrode, platinum (Pt) was the counter electrode and the sintered specimen functioned as the working electrode with a surface area of 1 cm^2. Cylindrical pins were made according to ASTM G99 specifications and tested at room temperature using a pin-on-disc wear tester (DUCOM, India). As the counterbody, EN 31(62 HRC) hardened steel was used. The wear parameters for all the specimens were taken as 900 m sliding distance, 20 N load, and 1 m/s sliding speed, then the wear rate was calculated using the equation given in [13]. The surface morphology of the SS316L-GNP composites before and after wear and corrosion testing were examined by means of a scanning electron microscope (Carl Zeiss, EVO MA10, Germany).

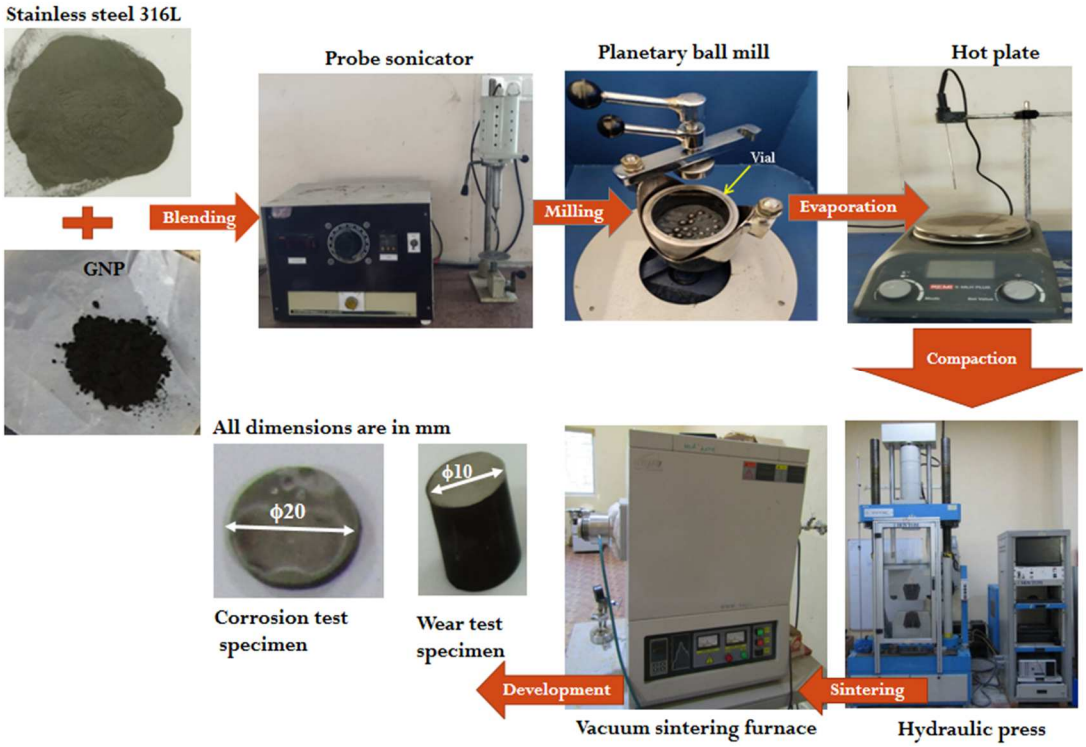

Fig. 1. Sequence of operations involved in development of composites

RESULTS AND DISCUSSION

Relative density, phases, and morphology of composites

Table 1 shows that as the GNP content was increased up to 0.5 wt.%, the relative densities of the composites grew for some extent, and afterwards decreased slightly for 0.75 wt.%. It means that there is no significant improvement in densification by an increase in GNP content. Because the powder particles were rearranged during sintering process by necking and grain boundary diffusion (one over the other) causes grain refinement [14].

TABLE 1. **Density, wear, and corrosion results of SS316L and SS316-xGNP (x: 0.25, 0.5 and 0.75 wt.%) composites**

Test	SS316L (a)	SS316L-GNP			Comparison (a)-(b)/(a)
		0.25 wt.%	0.5 wt.% (b)	0.75 wt.%	
Relative density [%]	97.45	97.54	97.61	97.11	5%↑
Hardness [HV]	134.50	270.10	289.70	282.60	115%↑
Wear rate ($x10^{-5}$ mm^3/Nm)	2.14	1.66	1.21	1.74	43%↓
Coefficient of friction	0.47	0.44	0.39	0.45	17%↓
E_{corr} [V]	–397.00	–274.00	–152.00	–288.00	--
I_{corr} ($x10^{-8}$ A/Cm^2)	43.60	2.09	0.93	19.70	--
Corrosion rate ($x10^{-2}$MPY)	20.00	0.96	0.43	9.00	98%↓

Another reason is that higher sintering temperatures, i.e. liquidus temperatures (>1400 °C) [14]. As the powders were compacted at liquidus temperatures (> 1400 °C), they form a liquid phase that induces capillary stress. This enables the spread of the liquid phase to the grain boundaries causing the filling of pores, thereby improving the densification [15]. Figure 2a shows the XRD spectrum of the SS316L-GNP (0.5 wt.% and 0.75 wt.%) milled powder and the composites in as-sintered conditions. No traces of GNP were detected in the milled powder or sintered specimens because GNP was used in small amounts. The reason might be that owing to the low scattering effect of carbon, XRD does not produce peaks (compared to SS) when used in lower proportions [16]. The as-sintered SS316L was characterized by an austenite phase with 2θ values of 44°, 51°, and 75° as confirmed by COD card no: 9015774. Nevertheless, M_7C_3 (M: Cr) carbides were detected with JCPDS card no. 00-036-1482 by increasing GNP to 0.75 wt.%. These carbids were produced by reacting GNP with Cr in SS316L. As the GNP content is increased (> 0.5 wt.%), different intermetallic compounds formed in the matrix, as reported by other researchers [17-19]. As seen in SEM micrograph (Fig. 2b), the GNP were pinned at the grain boundaries of the SS matrix to hinder grain growth, thereby a refined grain structure was produced in the as-sintered SS316L-0.5 wt.% GNP composite. Nonetheless, raising the GNP content beyond 0.5 wt.% causes agglomeration and grain coarsening of austenite, as published in the authors' previous work [12].

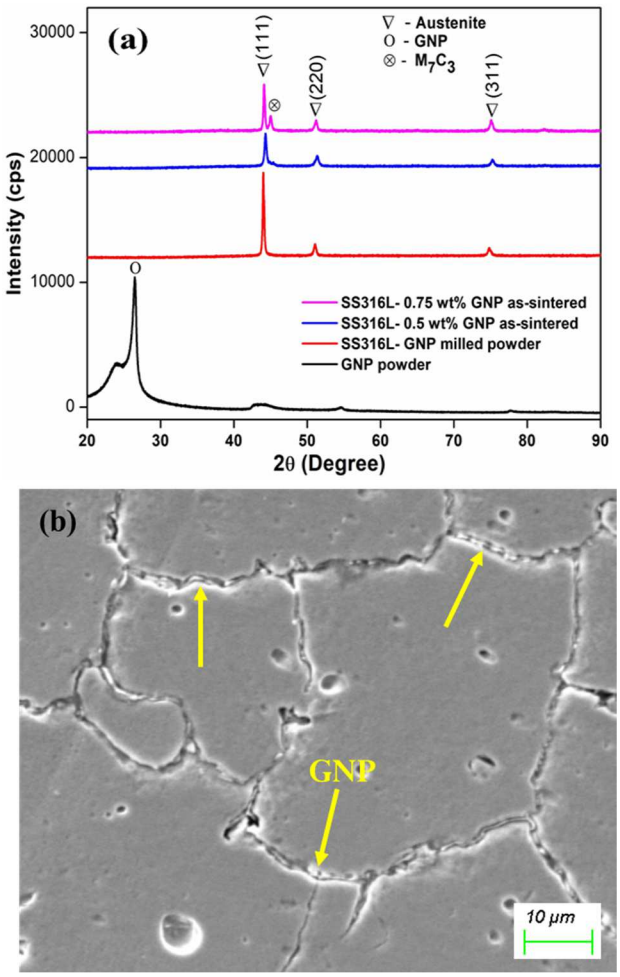

Fig. 2. a) XRD spectrum of SS316L-xGNP composites (0.5 wt.% and 0.75 wt.%), b) SEM micrograph of SS316L-0.5 wt.% GNP composite

Wear rate

The average hardness values of SS316L and the SS316L-xGNP (x: 0.25 wt.%, 0.5 wt.%, 0.75 wt.%) composites were obtained as 134.50, 270.10, 289.70, and 282.60 HV, respectively, before conducting the wear test. The coefficients of friction determined as a function of sliding distance for the SS316L, SS316L-xGNP (0.25 wt.%, 0.5 wt.%, and 0.75 wt.%) composite specimens is shown in Figure 3a. Initially, the coefficient of friction rapidly increased from 0 to the highest value for the base SS316L, and afterwards it stabilized. In the case of the SS316L-GNP (0.25 wt.%, 0.5 wt.%) composite specimens, the coefficient of friction was lower compared to the base SS316L. Afterwards, it moved to a steady state. The coefficient of friction for the 0.75 wt.% GNP specimen was slightly higher compared to the 0.5 wt.% GNP one.

The average coefficients of friction of SS316L and SS316L with varying xGNP wt.% (x: 0.25, 0.5, 0.75) composites were found to be 0.47, 0.44, 0.39,

and 0.45 respectively. The same trend in the wear rate was observed in all the specimens as shown in Figure 3b.

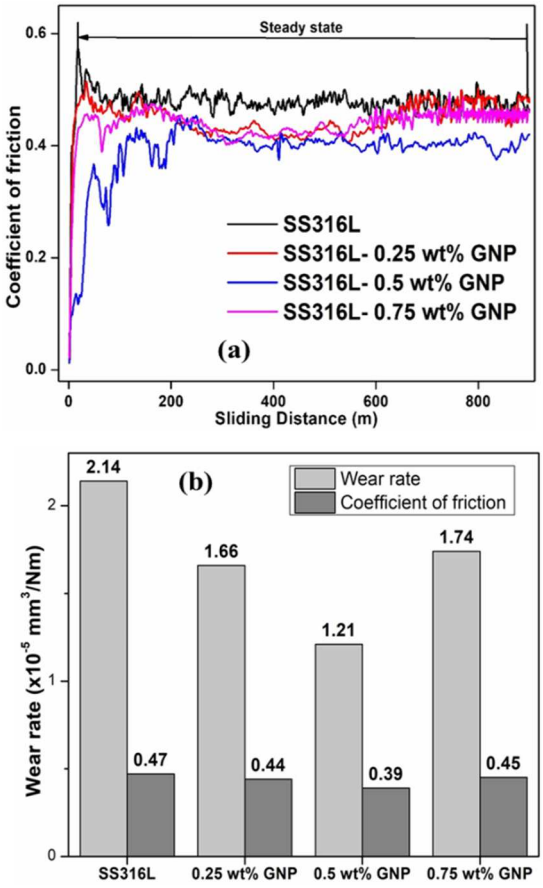

Fig. 3. Variation in coefficient of friction with sliding distance (a), wear rate for different GNP contents (b)

The wear rate decreases by introducing GNP to SS 316L at contents of 0.25 wt.% and 0.5 wt.%. Owing to the self-lubricating property and the high hardness of GNP, the wear resistance of the GNP-reinforced composites improved. However, the wear resistance increases with hardness according to the Archard equation [14, 20]. While conducting the wear test, the GNP comes out when the composite pin comes into contact with the counterbody, thus forming a black layer. This layer is called the self-lubricating film. This film is very soft and that reduces the contact between the pin and counterbody, which further lowers the COF. The wear rate increased at 0.75 wt.% GNP due to the coarser grain structure, which was explained in work [12].

Worn surface analysis

Figure 4 presents the SEM micrographs of the worn surfaces of the base SS316L and the composites with the addition of 0.25, 0.5, and 0.75 wt.% GNP. Figure 4a shows longer and wider grooves (WD) and micropits (MP) (indicated with yellow color) in the base SS316L specimen, which arose during sliding due to abrasive wear or ploughing action [21]. Nevertheless, it is believed that the presence of GNP in the composites causes a change in the wear mechanism.

Figure 4b and c shows the inclusion of 0.25, 0.5 wt.% GNP in SS316L, in which the grooves were reduced while smooth and finer tracks with no debris formation were observed owing to the formation of a protective layer by the self-lubricating nature of the GNP. This layer is called tribofilm as shown in Figure 4e.

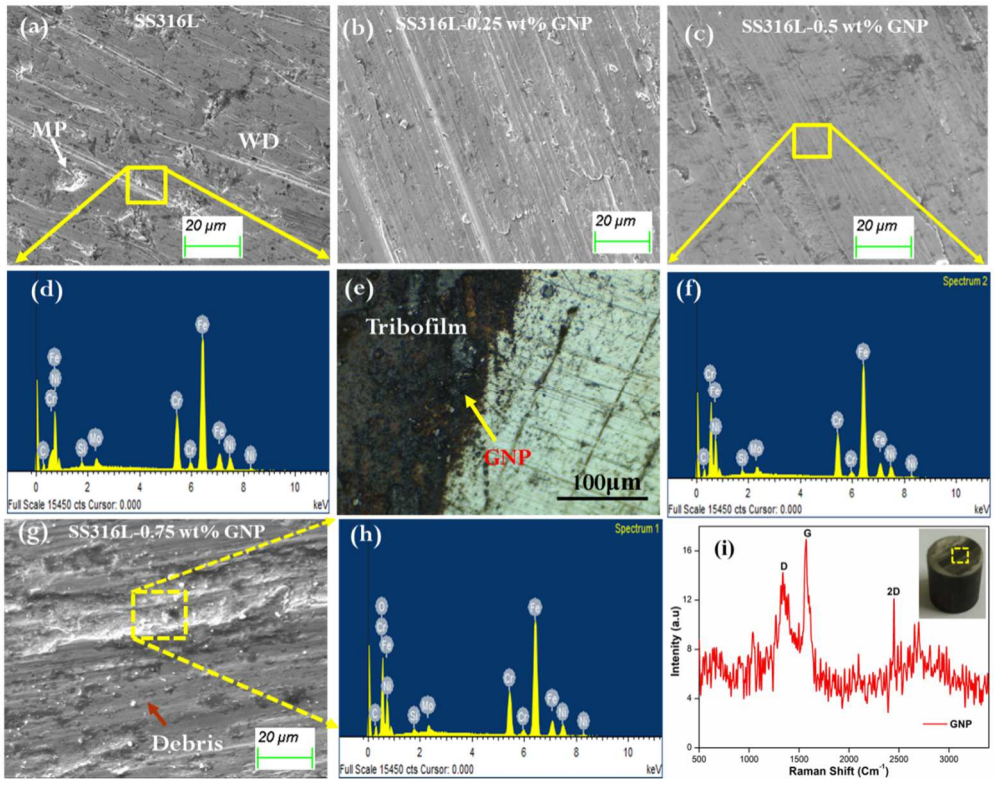

Fig. 4. Worn surface analysis of base SS316L and composite specimens (a-i)

The Raman spectroscopy technique was employed to identify GNP on the worn surfaces. Figure 4i shows the Raman spectrum comprised of three bands of D (1342 cm^{-1}), G (1570-1580 cm^{-1}), and 2D (2682 cm^{-1}), respectively. This indicates that the tribofilm protected the surface from ploughing and adhesive wear regimes and furthermore, the COF and wear rate of the composites were reduced. Figure 4g reveals that a significant amount of debris and material adhesion causes adhesive wear on the wear track surface. This is because of the poor wettability between the GNP and the matrix, which leads to more debris formation during the wear test. This debris acts like a third body and adheres to the contact surface, which contributes to a higher coefficient of friction and wear rate [14]. Table 2 displays the EDS results for the surfaces after the wear test at a 20 N load. The base 316L steel had large amounts of Fe, Cr, and Ni resulting from the abrasion mechanism [10]. The carbon content is greater as a consequence of increasing the amount of GNP. The amount of oxygen (oxidation) might have contributed to reducing the wear resistance when the GNP concentration was increased to 0.75 wt.% [11].

TABLE 2. **Elemental composition of worn composite surfaces**

Element	Composition [wt.%]						
	FeK	CrK	NiK	CK	OK	MoK	SiK
SS316L	67.97	14.93	8.29	3.45	--	2.31	--
SS316L-0.5 wt.% GNP	61.91	13.76	9.37	8.96	--	2.79	0.73
SS316L-0.75 wt.% GNP	50.59	11.96	7.47	10.28	18.48	2.07	0.47

Corrosion behavior

Figure 5a shows the potentiodynamic polarization plots of the SS316L-xGNP (x: 0.25, 0.5, 0.75 wt.%) composites in a 3.5 wt.% NaCl solution. It was observed that the anodic passive current densities (I_{corr}) were decreased by varying the GNP content up to 0.5 wt.%. The corrosion rate (CR) for all the composites, obtained by the Tafel extrapolation technique, is shown in Table 1.

It was observed that the corrosion potential and corrosion current density for the SS316L-0.5 wt.% GNP composite (E_{corr} = –152 mV, I_{corr} = 9.38E-9 A/cm^2) were lower than those of SS316L-0.75 wt.% GNP composites (E_{corr} = –288 mV, I_{corr} = 1.97E-7 A/cm^2). By varying GNP content up to 0.5 wt.%, the E_{corr} values got increased from –0.39 mV to –0.15 mV. Significantly the I_{corr} values decreased for the 0.25 and 0.5 wt.% GNP specimens than base SS316L. The corrosion potentials (E_{corr}) shifted towards positive values of 0.39, 0.27, 0.15 mV, indiating that a lower tendency of corrosion than the other specimens. The polarization curve for SS316L shifted downward compared to the others and it was also corroded. Hence, the 0.5 wt.% GNP composite exhibited the lowest corrosion rate of 0.0043 mils per year compared to all the samples presented in Figure 5b. It meant that the 0.5 wt.% GNP addition helps to decrease the corrosion rate.

There are different reasons why the corrosion resistance for the 0.25 wt.% and 0.5 wt.% GNP specimens is enchanced in relation to the base SS316L. Firstly, the GNP acts as a corrosion barrier with its high electron density, which slows down the ionic transfer between the corrosion medium (NaCl) and its reaction with the metal surface. The higher relative density of the specimens produced without porosity and voids plays an important role, reducing the microgalvanic reactions, which in turn increases the corrosion resistance [22-24]. Secondly, the Cr-carbide formation can also decrease the corrosion resistance [25]. The aluminides reinforced in the SS316L composites at the supersolidus temperature contributed to higher wear and corrosion behavior reported by Balaji et al. [9]. The rising I_{corr} values for the 0.75 wt.% GNP composite indicate a lower relative density, which is shown in Table 1.

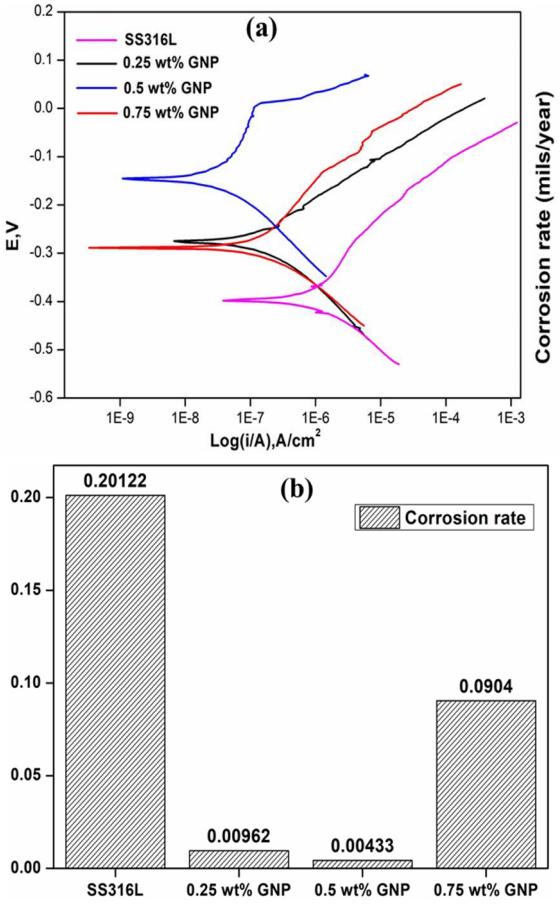

Fig. 5. Corrosion behavior (a), corrosion rate of SS316 (b) and SS316L-xGNP (x: 0.25, 0.5, 0.75 wt.%) composites

Corrosion morphology

The SEM morphology of all the specimens before and after the corrosion test is shown in Figure 6. Pitting

corrosion was observed to be significantly dependent on the porosity but not on the grain size. Pitting corrosion was regularly observed on the sub-surface pores. The base SS316L specimen containing a moderate level of porosity was consequently prone to pitting. Shallow pits were found (indicated with yellow arrows) with a size of approximately 10 µm. The SS316L-0.25 wt.% GNP composite specimen contains a low level of porosity and exhibits the initiation of pitting. The formed pits were smaller in size, less than 5 µm. The grain boundaries are clearly visible in the SS316L-0.5 wt.% GNP composite specimen. Pitting and clustering mechanisms were not found for 0.5 wt.% GNP. Furthermore, the SS316L-0.75 wt.% GNP composite was severely affected by intergranular corrosion (IGC) at the grain boundaries and pitting corrosion was hardly found. IGC is predominantly localized corrosion that occurs where the surrounding areas are depleted by carbide (Cr_7C_3) formation. This mechanism would be more influenced by the reduction in the mechanical and corrosion properties. The corroded region progressively increases from 5 µm to 25 µm for the SS316L-0.75 wt.% GNP composite. Another reason is that the SS316L-0.75 wt.% GNP composite specimen has a smaller relative density. It is logical to assume that it could have larger pores, rendering it more prone to pitting, as explained in Table 1. Finally, the rising corrosion potential (E_{corr} = –288.00 V) and passive current density (I_{corr} =1.97E-7 A/cm^2) are responsible for the growing corrosion rate at 0.75 wt.% [26].

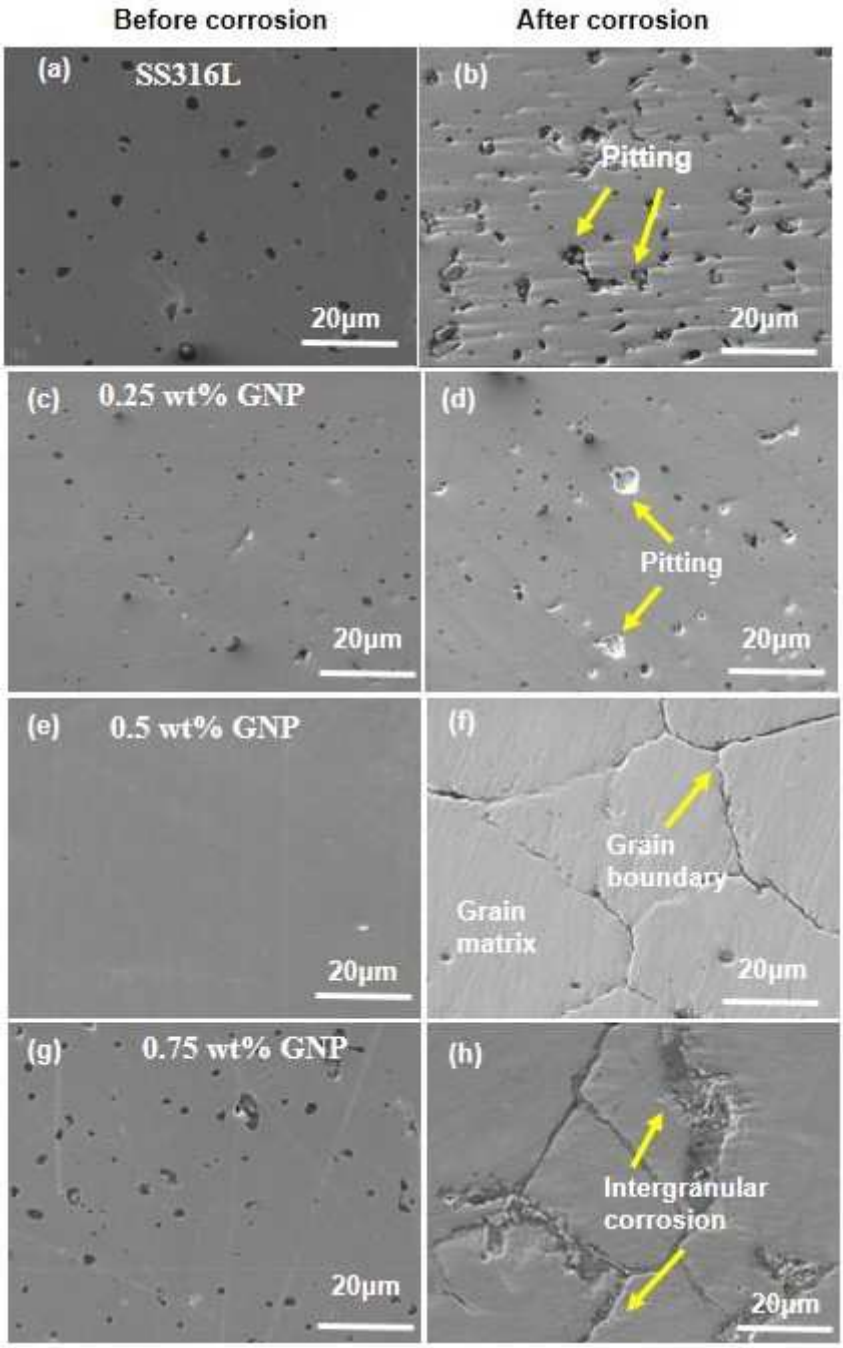

Fig. 6. Corrosion morphology of all composites

CONCLUSIONS

The present study was focused on the development of SS316L composites by employing GNP as the reinforcement at the liquidus temperature of 1400 °C for a holding time of 90 min. The major findings are summarized as follows:

- The relative density of the SS316L-0.5 wt.% GNP composites increased by 5% compared to the base SS316L and the other composites. The microstructure of SS316L was refined by reinforcing with 0.5 wt.% GNP, which hinders matrix grain growth due to the pinning mechanism.
- Owing to the self-lubricating effect of GNP, the wear rate and coefficient of friction of the SS316L-0.5 wt.% GNP composites were significantly reduced compared to other the composites by forming a tribofilm.
- The SS316L-0.5 wt.% GNP composite is strongly corrosion resistant compared to the other composites because of the higher relative density and lower passivation behavior.
- By means of the Tafel extrapolation technique, it was found that the corrosion rate decreased from 0.2 mils per year to 0.0043 mils per year for the SS316L-0.5 wt.% GNP composite in comparison to the base SS316L.

REFERENCES

[1] Wongpanya P., Pintitraratibodee N., Thumanu K., Euaruksakul C., Improvement of corrosion resistance and biocompatibility of 316L stainless steel for joint replacement application by Ti-doped and Ti-interlayered DLC films, Surf. Coatings Technol. 2021, 425, 127734, DOI: 10.1016/j.surfcoat.2021.127734.

[2] Sinha R.K., Nagpal Y., Sharma R., Kumar N., Investigation on corrosion characteristics of SS316L by thermal spray coating technique using Ni-80Cr alloy, J. Phys. Conf. Ser. 2022, 2178(1), DOI: 10.1088/1742-6596/2178/1/012032.

[3] Al-Mangour B., Mongrain R., Irissou E., Yue S., Improving the strength and corrosion resistance of 316L stainless steel for biomedical applications using cold spray, Surf. Coatings Technol. 2013, 216, 297-307, DOI: 10.1016/j.surfcoat.2012.11.061.

[4] Kuforiji C., Nganbe M., Powder metallurgy fabrication, characterization and wear assessment of SS316L-Al_2O_3 composites, Tribol. Int. 2019, 130, 339-351, DOI: 10.1016 / j.triboint. 2018.10.002.

[5] Padmavathi C., Upadhyaya A., Agrawal D., Corrosion behavior of microwave-sintered austenitic stainless steel composites, Scr. Mater. 2007, 57(7), 651-654, DOI: 10.1016/j.scriptamat.2007.06.007.

[6] Mahathanabodee S., Palathai T., Raadnui S., Tongsri R., Sombatsompop N., Dry sliding wear behavior of SS316L composites containing h-BN and MoS_2 solid lubricants, Wear [Internet] 2014, 316(1-2), 37-48, DOI: 10.1016/j.wear.2014.04.015.

[7] Kumar S.S., Sandeep E.S., Chandrasekhar S.B., Karak S.K., Development of nano-oxide dispersed 304L steels by mechanical milling and conventional sintering, Mater. Res. 2016, 19(1), 175-182, DOI: 10.1590/1980-5373-mr-2015-0593.

[8] Zou Y., Tan C., Qiu Z., Ma W., Kuang M., Zeng D., Additively manufactured SiC-reinforced stainless steel with excellent strength and wear resistance, Addit. Manuf. 2021, 41, March, 101971, DOI: 10.1016/j.addma.2021.101971.

[9] Balaji S., Vijay P., Upadhyaya A., Effect of sintering temperature on the electrochemical, hardness, and tribological properties of aluminide-reinforced austenitic stainless steel, Scr. Mater. 2007, 56(12), 1063-1066, DOI: 10.1016/j.scriptamat.2007.02.033.

[10] Zengin E., Ahlatci H., Zengin H., Investigation of microstructure, tribological and corrosion properties of AISI 316 L stainless steel matrix composites reinforced by carbon nanotubes, Mater. Today Commun. 2021, 29, December, 102758, DOI: 10.1016/j.mtcomm.2021.102758.

[11] Radhamani A.V., Lau H.C., Kamaraj M., Ramakrishna S., Structural, mechanical and tribological investigations of CNT-316 stainless steel nanocomposites processed via spark plasma sintering, Tribol. Int. 2020, 152, July, 106524, DOI: 10.1016/j.triboint.2020.106524.

[12] Kalyanamanohar V., Gopalakrishna A., Effect of SiC coated GNP on microstructure and mechanical properties of pressureless sintered SS316L composites, i-manager's, J. Mech. Eng. 2022, 12(3), 1, DOI: 10.26634/jme.12.3.18589.

[13] Veeramallu K., Gopala Krishna A., Friction stir processed Al 7075 matrix composites with addition of SiC coated graphene nanoplatelets, Mater. Today Proc. 2022, 56, 1594-9, DOI: 10.1016/j.matpr.2022.02.650.

[14] Mandal A., Tiwari J.K., AlMangour B., Sathish N., Kumar S., Kamaraj M., et al., Tribological behavior of graphene-reinforced 316L stainless-steel composite prepared via selective laser melting, Tribol. Int. 2020, 151, May, 106525, DOI: 10.1016/j.triboint.2020.106525.

[15] Kandala S.R., Balani K., Upadhyaya A., Mechanical and electrochemical characterization of supersolidus sintered austenitic stainless steel (316 L), High Temp. Mater. Process. 2019, 38(2019), 792-805, DOI: 10.1515/htmp-2019-0032.

[16] Khanna V., Kumar V., Bansal S.A., Prakash C., Ubaidullah M., Shaikh S.F., et al., Fabrication of efficient aluminium/graphene nanosheets (Al-GNP) composite by powder metallurgy for strength applications, J. Mater. Res. Technol. 2023, 22, 3402-3412, DOI: 10.1016/ j.jmrt.2022.12.161.

[17] Hooshmand Zaferani S., Ghomashchi R., Vashaee D., Thermoelectric, magnetic, and mechanical characteristics of antiferromagnetic manganese telluride reinforced with graphene nanoplates, Adv. Eng. Mater. 2021, 23(2), 1-9.

[18] Leng J-feng, Zhou Q-bo, Li Z-zhi, Dong Y-fan, Xia C-peng, Effect of graphene on microstructure and properties of Gr/CuCr10 composites, Trans. Nonferrous Met. Soc. China (English Ed.) 2022, 32(4), 1217-1225, DOI: 10.1002/adem.202000816.

[19] Kumar N., Lokesh K.S., Kannantha V., Pai R., Hebbale A.M., Development and experimental investigation of mechanical properties of graphene-based aluminum 6061 alloys, Mater. Today Proc. 2021, 46(7), 2421-2424, DOI: 10.1016/j.matpr.2021.01.303.

[20] Mandal A., Tiwari J.K., AlMangour B., Das A., Sathish N., Sharma R.K. et al., Microstructural and thermal expansion behaviour of graphene reinforced 316L stainless steel matrix composite prepared via powder bed fusion additive manufacturing, Results Mater. 2021, 11, 100200, DOI: 10.1016/j.rinma.2021.100200.

[21] Ouyang W., Xu Z., Jia S., Zhang M., Ye Y., Jiao J. et al., Multilayer-graphene reinforced 316L matrix composites preparation by laser deposited additive manufacturing: Microstructure and mechanical property analysis, Mater. Res. Express. 2019, July, 12, 6(9), DOI: 10.1088/2053-1591/ab2f2e.

[22] Chu K., Jia C., Enhanced strength in bulk graphene-copper composites, Phys. Status Solidi. Appl. Mater. Sci. 2014, 211(1), 184-190, DOI: 10.1002/pssa.201330051.

[23] Cunha A., Ferreira R., Trindade B., Silva F.S., Carvalho O., Production of a laser textured 316L stainless steel reinforced with CuCoBe + diamond composites by hot pressing: Influence of diamond particle size on the hardness and tribological behaviour, Tribol. Int. 2020, 146, 106056, DOI: 10.1016/j.triboint.2019.106056.

[24] Veeresh Nayak C., Ramesh M., Desai V., Kumar S.S., Fabrication of stainless steel based composite by metal injection moulding, Mater. Today Proc. 2018, 5(2), 6805--6814, DOI: 10. 1016/j.matpr.2017.11.340.

[25] Kumar V., Joshi P., Dhakar S., Analysis of the effect of sensitization on austenitic stainless steel 304L welded by GTAW process, HCTL Open Int. J. Technol. Innov. Res. 2015, 14, August, 978-979.

[26] Yao Y., Miao S., Liu S., Ma L.P., Sun H., Wang S., Synthesis, characterization, and adsorption properties of magnetic Fe_3O_4@graphene nanocomposite, Chem. Eng. J. 2012, 184, 326-332, DOI: 10.1016/j.cej.2011.12.017.

